Available online at www.sciencedirect.com
ScienceDirect
Journal of the European Ceramic Society 30 (2010) 819–829
www.elsevier.com/locate/jeurceramsoc

Influence of microporosity and macroporosity on the mechanical properties of biphasic calcium phosphate bioceramics: Modelling and experiment

F. Pecqueux [a,b,1,2], F. Tancret [a,*], N. Payraudeau [a,b,1,2], J.M. Bouler [b,2]

[a] *Université de Nantes, Laboratoire Génie des Matériaux et Procédés Associés, Polytech'Nantes La Chantrerie, BP 50609, 44306 Nantes Cedex 3, France*
[b] *INSERM UMR 791, Ingénierie Ostéo-Articulaire et Dentaire, Université de Nantes 1, place Alexis Ricordeau, BP 84215, 44042 Nantes Cedex 1, France*

Received 15 June 2009; received in revised form 25 August 2009; accepted 10 September 2009
Available online 20 October 2009

Abstract

Macroporous biphasic calcium phosphate (BCP) bioceramics, for bone substitution applications, have been synthesized, cold isostatically pressed and pressureless sintered, using naphthalene particles as a porogen to produce macropores. The resulting materials are mixtures of β-tricalcium phosphate and hydroxyapatite with various microporosities and macroporosities. Mechanical properties (Young's modulus, compressive strength and fracture toughness) were measured on specimens over the widest attainable ranges of porosities, and compared to previously proposed analytical models and hypotheses. These models describe the evolution of the mechanical properties as functions of macroporosity and microporosity separately, the strength model considering macropores as critical flaws in the ceramic. Results show that the presence of macropores strongly influences the critical flaw size, but the latter appears to increase with macroporosity. This phenomenon can be explained by the presence of clusters of macropores, acting as critical flaws, becoming larger as macroporosity increases.

Keywords: Fracture stress; Apatite; Microstructure; TCP; Modeling

1. Introduction

Since 1920,[1] calcium phosphate ceramics have been used as bone substitutes[2–5] because their chemical composition is close enough to the one of the mineral part of bones,[6,7] so that they can be recognized, dissolved and remodelled as new bone tissues by specific cells. Among them, the biphasic calcium phosphates (BCP), that are mixtures of hydroxyapatite (HA), $Ca_{10}(PO_4)_6(OH)_2$, and β-tri-calcium phosphate (β-TCP), $Ca_3(PO_4)_2$, are of particular interest. The choice of the ratio between HA and β-TCP allows to control their dissolution rate.[8–10] Also, the mechanical properties of the BCP mixture were shown to be higher than those of the single phases.[11]

To optimize their biological efficiency, these synthetic bone substitutes require a particular porous microstructure combining macroporosity (isolated or interconnected pores larger than 100 μm, generally generated by the elimination of porogens) and microporosity (interstitial spaces remaining between the grains of the ceramic matrix after an incomplete sintering, typically of the order of a micrometer).[12] However, mechanical properties are greatly reduced by the introduction of these porosities,[13,14] excluding the use of these ceramics for load-bearing applications. Mechanical properties can also be modified by parameters like the ratio HA/TCP,[14,15] the grain size,[15,16] or a chemical doping,[17,18] etc., but the effect of porosity is by far more important than all other factors. In view of possible load-bearing applications, it is therefore important to fully characterise the mechanical behaviour of porous BCP ceramics, and to describe their dependence on porosity as accurately as possible with appropriate models.

In a number of studies, the mechanical properties of calcium phosphate ceramics have been investigated as a function of their microporosity[14,16,19] (or sintering temperature[11,15]),

* Corresponding author. Tel.: +33 240683197; fax: +33 240683199.
E-mail addresses: francois.pecqueux@univ-nantes.fr (F. Pecqueux), franck.tancret@univ-nantes.fr (F. Tancret), jean-michel.bouler@univ-nantes.fr (J.M. Bouler).
[1] Tel.: +33 240683197; fax: +33 240683199.
[2] Tel.: +33 240084616; fax: +33 240083712.

0955-2219/$ – see front matter © 2009 Elsevier Ltd. All rights reserved.
doi:10.1016/j.jeurceramsoc.2009.09.017

their macroporosity,[12,20] or their total porosity[14,21] but only a few made the distinction between these two types of porosity.[13,14,22,23] Among these studies, only some described the influence of porosities by more or less empirical mathematical equations:

- De Groot used exponential laws to describe the variations of compressive and tensile strengths of HA and β-whitlockite (β-TCP) respectively as functions of total porosity (from 0% to 50%) and microporosity (from 0% to 5%).[14]
- Bignon et al. used the same type of law to describe the variations of BCP compressive strength as a function of macroporosity (from 0% to 65% of porogen volume fraction).[22]
- Zhang et al. used a power law to describe the variations of Young's and shear moduli of calcium phosphate cements as a function of porosity (from 0% to 75% of porogen volume fraction).[20]
- Le Huec et al.[23] described the contribution of macroporosity (from 0% to 28% of the specimen volume occupied by pores larger than 100 μm in diameter) and microporosity (from 22% to 39% of the specimen volume occupied by pores smaller than 100 μm in diameter) to the compressive strength of HA using empirical polynomial regressions.
- Bouler et al.[13] fitted the variations of the compressive strength of BCP with polynomial regressions. They studied the influence of five parameters: HA weight percentage in the BCP starting powder (45%, 60% and 75%), isostatic compaction pressure, weight percentage (30%, 45% and 60%) and mean size of naphthalene particles (related to the macropore sizes and proportion), and final sintering temperature (900, 1000 and 1100 °C, linked to the remaining microporosity).

In addition to these experimental observations, several types of models were previously proposed to describe the variations of mechanical properties of materials as functions of porosity. Some of the proposed approaches are discussed hereafter: initially, the behaviour of ceramic materials containing a limited porosity was empirically described by linear laws[24,25] but even if the approximation is sufficient for low porosities it becomes inaccurate for highly porous materials. Then, different ways to consider the porosity, its morphology and its influence on mechanical properties were proposed, which led to various models. The first approach, derived from homogenisation methods,[26–28] was to assume that porous materials are special cases of biphasic materials with mechanical properties equal to zero for the "porous phase".[29–32] They generally lead to polynomial or homographic laws. The main drawback of such models is that they do not consider the morphology of porosity as being specific (it is just assumed to be identical to that of a composite microstructure which is actually made of two solid phases). One of its consequences is that such models are only equal to zero when the pore volume fraction is equal to one, which cannot hold in the case of porous materials obtained by the incomplete sintering of a pressed powder. Then, models considering the specific morphology of porous media were proposed. For instance, Gibson and Ashby[33] calculated a simplified mechanical response of cellular solids, and obtained a power-law dependence of the elastic modulus with relative density. Several other analyses led to various power laws, including parameters with different physical meanings.[34,35] Rice performed an interesting review work leading to the synthesis of several existing models into the "minimum solid area" (MSA) concept, showing that most models could be mathematically approximated in a common manner using exponential laws.[36,37] It was then demonstrated that this unified MSA methodology was adapted to describe the mechanical properties of porous microstructures presenting various morphologies (packings of grains densified by sintering, cellular materials containing closed pores, trabecular structures made of struts). Additionally, other models, based on morphological analyses taking into account (in a more or less explicit manner) the geometrical randomness of the pore structure, have also been proposed, either in the case of sintered bodies[38] or holding in the case of cellular and/or trabecular structures.[39] The majority of the previously mentioned approaches mainly considered elastic properties, although some studies also focused on fracture properties. In particular, on the basis of elastic fracture energy considerations, Wagh et al. described a procedure allowing to transpose elastic property models to fracture toughness and strength models.[40] This procedure was later corrected[41] and it was demonstrated that it could be generalized to any kind of porosity–property mathematical expressions.[42]

Another, more recent, approach consists in numerical simulation of porous microstructures using finite element modelling. Studies can be found for both elastic properties[43–45] and for fracture properties,[46,47] but they always address only one type of porosity morphology at a time.

In the light of the above-reviewed literature, it appears that a complete macroporosity–microporosity model, validated on the whole attainable ranges of both porosities, for elastic as well as fracture properties, is missing. Indeed, in the case of BCP ceramics, the most comprehensive experimental attempt to date is that of Le Huec et al.,[23] where both macroporosity and microporosity were varied. However, (i) the microporosity range was rather narrow (always higher than 20% of the total volume), (ii) only the compressive fracture stress was measured and (iii) empirical polynomial fits were used as mathematical descriptions of the strength as a function of porosities. On the modelling side, an approach was proposed by some of the present authors,[48] that could potentially be applied to several mechanical properties (Young's modulus, fracture toughness, fracture strength, hardness). However, it could not be completely validated due to a lack of available experimental data (only one macroporosity level was tested, and the investigated microporosity range was quite narrow): "such models will be completely validated only if additional measurements are provided, on extended ranges of macroporosity and microporosity".[48] The aim of the present work is precisely to provide more experimental measurements of several properties (Young's modulus, fracture toughness, compressive strength) on extended ranges of porosities (from a nearly dense body to materials with a total porosity of more than 70%), and to see if, in the light of these new data, adjustments to the

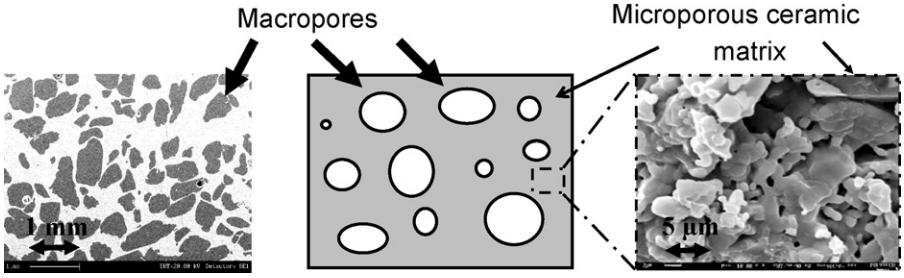

Fig. 1. Scanning electron micrographs and schema of the BCP porous structure.

modelling approach are necessary to fully capture the occurring physical phenomena.

2. Theoretical background

The base for our approach is a previously published model,[48] as stated in Section 1. Its construction is briefly described hereafter. The model considers that, given the huge difference in size between macropores (hundreds of micrometers) and micropores (micrometers), the material can be regarded as a quasi-continuous microporous "matrix" containing isolated macropores (Fig. 1). In this respect, it becomes possible to split the respective influence of macroporosity and microporosity. In particular, in the case of the Young's modulus, this writes[48]:

$$E = E_0 \cdot f_1(p_{\text{macro}}) \cdot f_2(p_{\text{micro}}) \tag{1}$$

with E the Young's modulus of the porous material and E_0 the value for a fully dense body. Respectively, f_1 and f_2 are functions of the macroporosity, p_{macro}, defined as the ratio of the macroporous volume over the total volume, and of the microporosity, p_{micro}, defined as the local porosity of the ceramic "matrix" situated between the macropores (this is why the sum $p_{\text{macro}} + p_{\text{micro}}$ can, theoretically, be higher than one).

The chosen model for macroporosity is that proposed by Wagh et al.,[39] since its mathematical formulation is well adapted to the case of isolated pores within a continuous matrix, *i.e.* it is equal to zero only when the material is fully porous. For a material with a porosity p, it writes:

$$E = E_0 \cdot (1 - p)^m \tag{2}$$

In our case, the "matrix" between macropores is itself microporous, and its local Young's modulus, E_m, is reduced by the presence of micropores compared to the bulk value, E_0. The above equation becomes then:

$$E = E_m \cdot (1 - p_{\text{macro}})^m \tag{3}$$

E_m is therefore the Young's modulus of a microporous ceramic whose porosity results from the incomplete sintering of a pressed powder. To describe its dependence on microporosity, the chosen model is that of Jernot et al.,[38] since it applies to partly sintered packings of grains:

$$E_m = E_0 \cdot [N_C \cdot (1 - p_{\text{micro}}) - (N_C - 1) \cdot (1 - p_{\text{micro}})^{2/3}] \tag{4}$$

where N_C, the mean coordination number, is the average number of closest neighbours of a given grain in the initial packing.

Combining the last two equations, this gives[48]:

$$E = E_0 \cdot [N_C \cdot (1 - p_{\text{micro}}) - (N_C - 1) \cdot (1 - p_{\text{micro}})^{2/3}] \cdot (1 - p_{\text{macro}})^m \tag{5}$$

The reported approach also proposed a model for fracture toughness, following a procedure established by Wagh et al.[40] and corrected by Arató.[41] This gives[48]:

$$K_{\text{IC}} = K_{\text{IC0}} \cdot [N_C \cdot (1 - p_{\text{micro}}) - (N_C - 1) \cdot (1 - p_{\text{micro}})^{2/3}] \cdot (1 - p_{\text{macro}})^m \tag{6}$$

where K_{IC0} is the toughness of a fully dense material, *i.e.* with $p_{\text{micro}} = p_{\text{macro}} = 0$.

Finally, after observing that the calculated critical flaw size was always of the order of the macropore size, it was assumed that a macropore was the critical flaw.[48] Given the large number of calibrated macropores contained in each specimen, it was considered that the critical flaw was always of similar shape and size. The classical relation between fracture toughness, strength and critical flaw size and shape was then used:

$$\sigma_r = \frac{K_{\text{IC}}}{Y \cdot \sqrt{a_C}} \tag{7}$$

with Y the geometrical factor associated to the critical flaw and a_C its size. If Y and a_C are constant, then:

$$\sigma_{r0} = \frac{K_{\text{IC0}}}{Y \cdot \sqrt{a_C}} \tag{8}$$

with σ_{r0} the virtual strength of the dense material, *i.e.* with $p_{\text{micro}} = p_{\text{macro}} = 0$. This led to the definition of a strength model, using the general expression of toughness as in Eq. (6). This gives:

$$\sigma_r = \frac{K_{\text{IC}}}{Y \cdot \sqrt{a_C}} = \frac{K_{\text{IC0}}}{Y \cdot \sqrt{a_C}} \cdot [N_C \cdot (1 - p_{\text{micro}}) - (N_C - 1) \cdot (1 - p_{\text{micro}})^{2/3}] \cdot (1 - p_{\text{macro}})^m \tag{9}$$

and finally[48]:

$$\sigma_r = \sigma_{r0} \cdot [N_C \cdot (1 - p_{\text{micro}}) - (N_C - 1) \cdot (1 - p_{\text{micro}})^{2/3}] \cdot (1 - p_{\text{macro}})^m \tag{10}$$

The aims of this work consist in validating the above models by measuring the three mechanical properties (E, K_{IC}, σ_r) over the widest possible ranges of microporosities and macroporosities and to test the above hypotheses, *i.e.*:

- The critical flaw is always a macropore.
- The analytical models (Eqs. (5), (6), (10)) can describe the variations of E, K_{IC} and σ_r with macroporosity and microporosity using the same values for the parameters N_C and m.

3. Materials and testing

3.1. Fabrication of materials

To make sure that the chemical composition and the granulometry of powders are controlled and reproducible, the powder used to fabricate all the specimens was synthesized in our laboratories. Two batches of Calcium Deficient Apatite (CDA) powders (referred to as CDA-A and CDA-B) have been synthesized by hydrolysis of commercial powders of di-calcium phosphate di-hydrated in an aqueous solution of NH_4OH maintained at 70 °C under vigorous stirring during 6 h. The initial pH and reactant stoichiometry were chosen to obtain a final atomic Ca/P ratio close to 1.52. The solutions were then filtered and dried at 120 °C for 12 h. The CDA powders were mixed with different proportions of naphthalene particles (previously sifted between 200 and 600 μm) using a Turbula shaker-mixer. The resulting mixtures were cold isostatically pressed under 140 MPa to form plates of around 12 mm in thickness. The plates were then heated at 80 °C during 48 h to sublimate the naphthalene particles, and subsequently pressureless sintered in air, following a controlled firing schedule: a heating in two steps (at the rate of 1 and 5 °C/min) and two plateaus (at 350 °C during 3 h to eliminate all residual traces of porogen and/or humidity and at temperatures between 850 and 1250 °C for 8 h) and a slow cooling at the rate of 1 °C/min to avoid the cracking of the plates. During sintering, the CDA transforms into a mixture of HA and β-TCP; the proportions of which were evaluated from the relative areas of the main peaks of each phase on standard X-ray diffractograms. The sintering of CDA-A leads to a BCP-A composed of 20% HA and 80% β-TCP while CDA-B leads to a BCP-B composed of 15% HA and 85% β-TCP. Infrared spectroscopy was also used to check the purity of materials.

To quantify porosities, small parallelepipedic blocks were cut out from each plate. Total porosity was estimated through the apparent density. Specimens were then impregnated under vacuum with an epoxy resin and polished with SiC papers down to grade P4000. Macroporosity was measured by quantitative image analysis on polished cross-sections.[49] The microporous volume is then obtained by subtracting the macroporous volume and the solid volume from the total volume. Microporosity is the ratio of the microporous volume over the difference between the total volume and the macroporous volume. The fabricated ceramics contain macroporosities ranging from 0% to 53% and microporosities comprised between 2% and 50%.

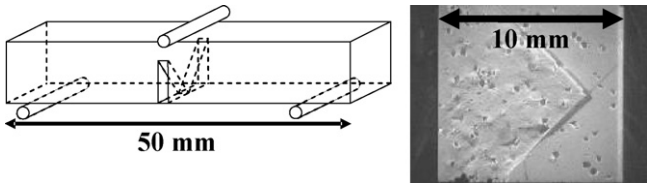

Fig. 2. Schema of a three-point bending toughness test and fractograph of a chevron notched bar.

3.2. Mechanical properties testing

The Young's modulus was measured in three-point bending on parallelepipedic bars of approximately 8 mm × 10 mm × 50 mm cut from plates of batch A (from one to three bars for each material). Deflection was measured using a Linear Variable Differential Transformer (LVDT), with a precision of less than a micrometer. Fracture toughness was tested following a procedure described by Dlouhy et al.,[50] in three-point bending on the same parallelepipedic bars (batch A) after introducing a chevron notch (Fig. 2). Compression tests were made on parallelepipedic blocks (~7 mm × 7 mm × 11 mm) that had been cut out from the plates of both batches (from three to seven blocks for each material).

4. Results and discussion

4.1. Fitting procedure

Several specimens have been mechanically tested for each couple of macroporosity and microporosity. Experimental results are plotted in different diagrams (Figs. 3–10) but, for clarity reasons, error bars are displayed only on the graphs comparing the measured and the calculated properties values (Figs. 4, 6, 8, 10). The extrema of error bars correspond to the minimum and maximum values measured. No error bar appears in the case of single measurements. The parameters of analytical models are then adjusted to obtain the best fit of experimental data, by minimising the sum of the absolute relative differences between measured and calculated values.

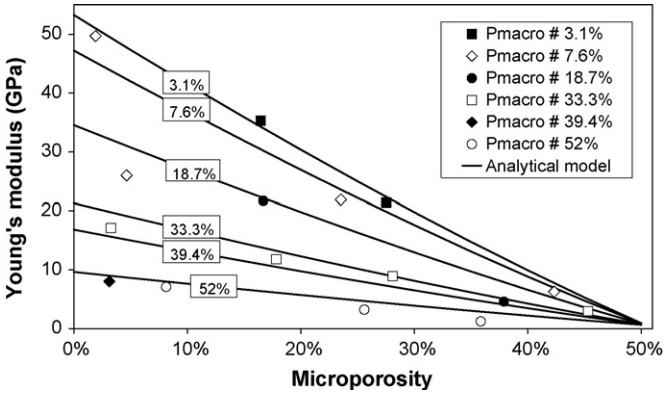

Fig. 3. Experimental and modelled Young's modulus as function of microporosity, for different macroporosities (batch A). Solid lines are calculated variations for given macroporosities.

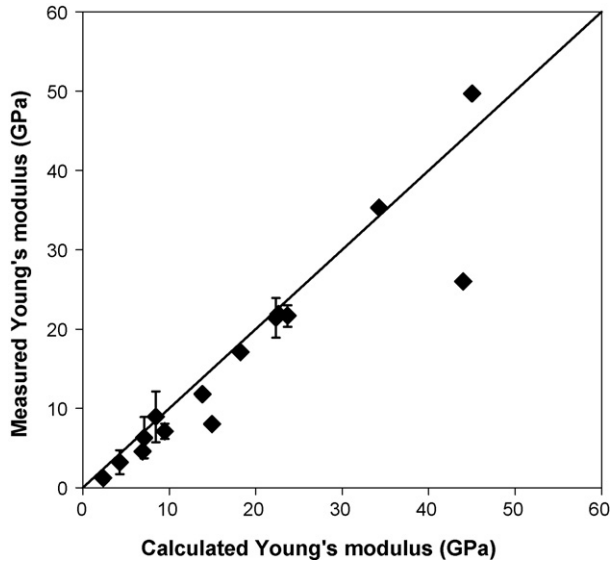

Fig. 4. Comparison between experimental and calculated values for Young's modulus (batch A).

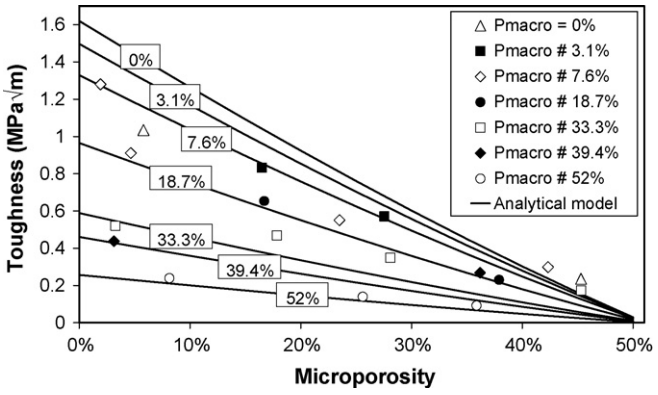

Fig. 5. Experimental and modelled toughness as function of microporosity, for different macroporosities (batch A). Solid lines are calculated variations for given macroporosities.

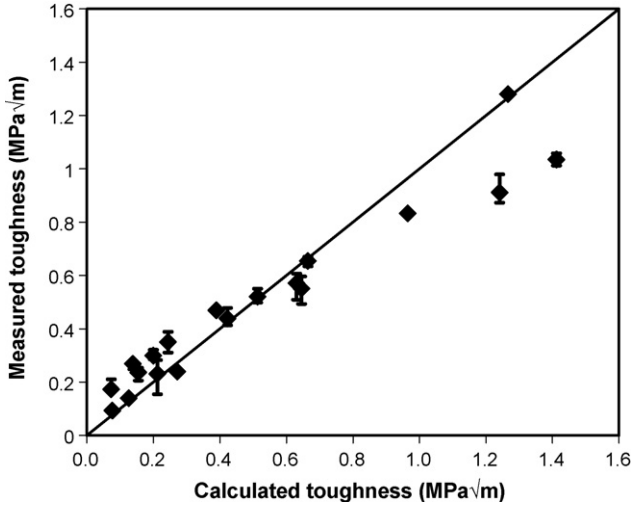

Fig. 6. Comparison between experimental and calculated values for toughness (batch A).

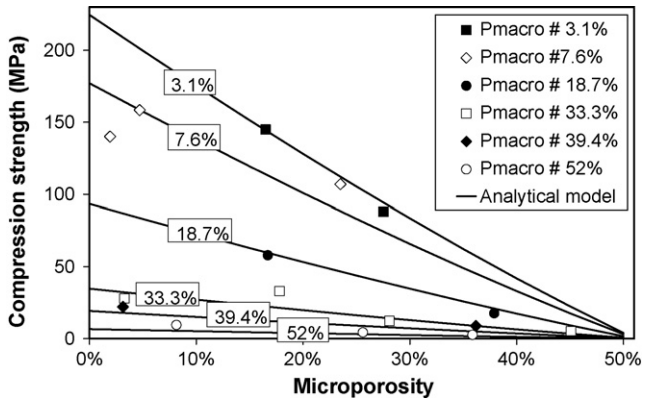

Fig. 7. Experimental and modelled compression strength as function of microporosity, for different macroporosities (batch A). Solid lines are calculated variations for given macroporosities.

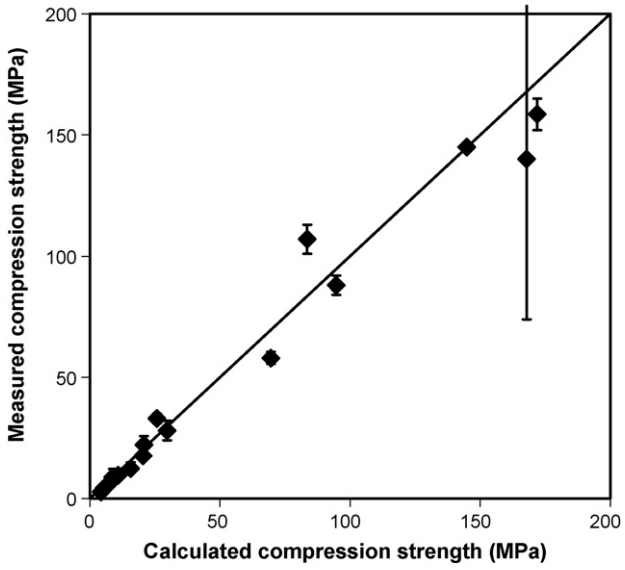

Fig. 8. Comparison between experimental and calculated values for compression strength (batch A).

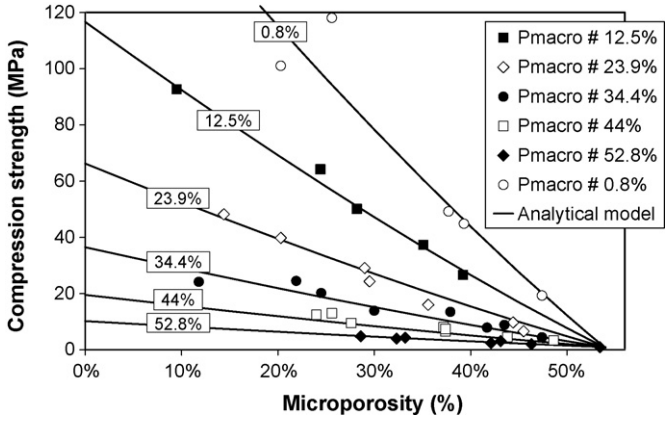

Fig. 9. Experimental and modelled compression strength as function of microporosity, for different macroporosities (batch B). Solid lines are calculated variations for given macroporosities.

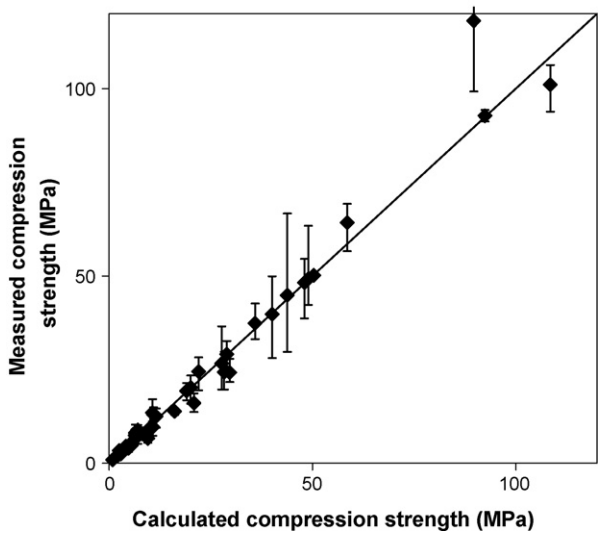

Fig. 10. Comparison between experimental and calculated values for compression strength (batch B).

However, at the beginning of the fitting procedure, it appeared that most curves did not tend towards zero for the microporosity of the pressed powder before sintering, as could be expected by the mathematical form of the models. Instead, it seemed that the curves would sometimes tend towards a fixed value. This might be explained by the fact that a pressed powder never has strictly null mechanical properties, even if extremely weak. But another explanation, in the case of BCP ceramics, is that materials experience a phase transformation during heating before reaching sintering temperatures (CDA transforms into a mixture of HA and β-TCP). This phenomenon, even if it does not generate any shrinkage, may produce small chemical contacts between the reacting crystals and, hence, non-negligible mechanical properties (resulting in the observed offset). To improve fitting, it was thus necessary to modify the models (Eqs. (5), (6), (10)) by adding a constant term (X_{min}) in each microporosity model (see Eqs. (11)–(13) in the next section). This minimum value corresponds to the mechanical property that would be measured on specimens cut in a microporous plate at the start of sintering, *i.e.* after the phase transformation and after a possible grain rearrangement, but before shrinkage.

4.2. Young's modulus model

In the case of the Young's modulus, the above model modification writes:

$$E = \{E_0 \cdot [N_C \cdot (1 - p_{micro}) - (N_C - 1) \cdot (1 - p_{micro})^{2/3}] + E_{min}\} \cdot (1 - p_{macro})^m \quad (11)$$

with $E_0 + E_{min}$ the Young's modulus of the fully dense material, *i.e.* with $p_{micro} = p_{macro} = 0$. The best description of experimental data has been obtained with $E_0 = 57$ GPa, $E_{min} = 0.6$ GPa, $N_C = 4.8$ and $m = 2.5$ (Fig. 3). The E_0 value is lower than values reported for dense BCP materials (for example $E_0 = 102$ MPa reported by Ruseska et al.[11]). That can be explained by the observation of microcracks in the specimens, decreasing their stiffness.[51] The other parameter values are close to those generally obtained for ceramic materials (N_C between 5 and 7 and m between 2 and 5).[38,39] Another way to display results is to plot the measured values as a function of the calculated ones. A fairly good agreement is obtained, as shown in Fig. 4. Only one measurement seems significantly lower than the calculated value; after careful binocular observation of the specimen, it appeared to contain several millimeter-sized cracks, probably originating from the fabrication process (cooling from sintering and/or machining), and certainly responsible for the low Young's modulus value.

4.3. Toughness model

Taking into account the suggested modification, the toughness model can be written:

$$K_{IC} = \{K_{IC0} \cdot [N_C \cdot (1 - p_{micro}) - (N_C - 1) \cdot (1 - p_{micro})^{2/3}] + K_{IC\,min}\} \cdot (1 - p_{macro})^m \quad (12)$$

where $K_{IC0} + K_{ICmin}$ is the toughness of the fully dense material, *i.e.* when $p_{micro} = p_{macro} = 0$. The best fit of the collected data has been found with $K_{IC0} = 1.6$ MPa $\sqrt{m}$, $K_{ICmin} = 0.02$ MPa $\sqrt{m}$, $N_C = 4.8$ and $m = 2.5$ (Fig. 5). Additionally, it must be noted that the same N_C and m values can be used to fit both the Young's modulus and the toughness, confirming the previously mentioned hypothesis. Once more, plotting the measured values as a function of the calculated ones provides further assessment of our model (Fig. 6).

4.4. Compression strength model

The fracture strength model, after introducing the offset modification, writes:

$$\sigma_r = \{\sigma_{r0}[N_C \cdot (1 - p_{micro}) - (N_C - 1) \cdot (1 - p_{micro})^{2/3}] + \sigma_{r\,min}\} \cdot (1 - p_{macro})^m \quad (13)$$

where $\sigma_{r0} + \sigma_{rmin}$ is the compressive strength of the fully dense material, *i.e.* when $p_{micro} = p_{macro} = 0$. For batch A, the best description of the experimental data has been obtained for $\sigma_{r0} = 260$ MPa, $\sigma_{rmin} = 3$ MPa, $N_C = 4.8$ and $m = 5$ (Fig. 7). A good fit is found between the measured and the calculated values (as shown on Fig. 8). In the case of batch B, the best fit has been found for $\sigma_{r0} = 190$ MPa, $\sigma_{rmin} = 2$ MPa, $N_C = 4.4$ and $m = 3.8$ (Fig. 9). A very good agreement is obtained between the measured and the calculated values, as shown in Fig. 10.

Nevertheless, although strength measurements can be described in a satisfactory manner by the analytical model, it should be noted that the values obtained for the parameter m (5 and 3.8 for batches A and B, respectively) are different from our values for Young's modulus and toughness. This is not consistent with our initial assumption that all three mechanical properties should be described by the same parameters N_C and m. It is the case for N_C, since the microporous structure is the same, but not for m. This will be discussed and investigated in the next section, on the basis of further experiments.

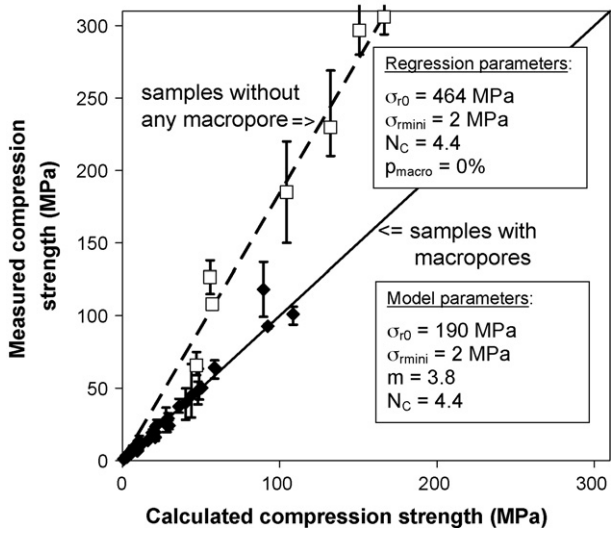

Fig. 11. Comparison between experimental and calculated values for compression strength (batch B).

4.5. Discussion: strength model and fracture mechanisms

The assumption that the strength could be described by the same type of model as for fracture toughness, using the same parameters N_C and m, was based on the hypothesis that the critical flaw was always a macropore, and hence always (approximately) of the same size and shape. In view of the present results, this hypothesis must be rejected, at least partly. Therefore, experiments were further analysed to investigate the origin of this discrepancy. Fig. 11 shows the comparison between calculated and measured strength values in the case of materials containing macropores (p_{macro} from 0.8% to 52.8%) and in the case of materials containing no macropore ($p_{macro} = 0$), all fabricated from the CDA-B powder. It can be seen that, although the fit is very good for the materials containing macropores, the model is not able to fit the data with the same values of σ_{r0} when the ceramics contain no macropore. Indeed, the fracture strength of materials with 0% macroporosity appears to be about twice higher than the calculated one. It is nevertheless possible to obtain a good fit of the experimental strength of the material containing no macropore by changing the parameter value σ_{r0} to 464 MPa and with $p_{macro} = 0$. This indicates that the model is still valid, but that the critical flaw is smaller in the materials containing no macropore than in the macroporous ceramics. This observation indicates that the critical flaw is linked to the presence of macropores as soon as the latter are present in the ceramic. The original assumption may, therefore, not be completely wrong.

Other experiments were made to try and confirm the hypothesis. Small bars containing no macropore or a single naphthalene particle, placed in different locations, were fabricated. After the naphthalene sublimation heat treatment (to create a single macropore) and sintering, the bars were broken in three-point bending (Fig. 12). For each bar containing no macropore, or even a macropore situated in a "low stress" location, the fracture always occurred at the vertical of the central loading point (*i.e.* in the highest stress area). However, for the bars containing a single macropore in a highly stressed area (*i.e.* close to the vertical of the loading point and close to the lower surface of the specimen), fracture always occurred through the macropore, even if it was not exactly placed below the loading point. The shift of the rupture location in such cases indicates that in these specimens, the fracture initiated from the macropore, hence acting as the critical flaw. This observation also tends to confirm that macropores, when present, can constitute the critical flaws. The above two experiments would tend to confirm the original hypothesis (that a macropore is always the critical flaw), but do not explain the observed discrepancy in the case of the fracture strength model. To explain it, let us remind the hypothesis: a macropore always being the critical flaw, the latter has always (approximately) the same shape and size and therefore the same parameter m can be used for both toughness and strength (expressed by Eqs. (6)–(10)). However, if we calculate for our ceramics the quantity $(K_{IC}/\sigma_r)^2$, which is proportional to the critical flaw size (as defined in Eq. (7)), it appears that this size globally increases with macroporosity, as shown in Fig. 13. This observation contradicts the above-mentioned hypothesis, *i.e.* the critical flaw is not constant in size. Thus, assuming that it is possible to describe the variation of the critical flaw size with a function of macroporosity g, as $a_C = a_{C0}g(p_{macro})$, from a mathematical point of view, Eq. (9) rewrites:

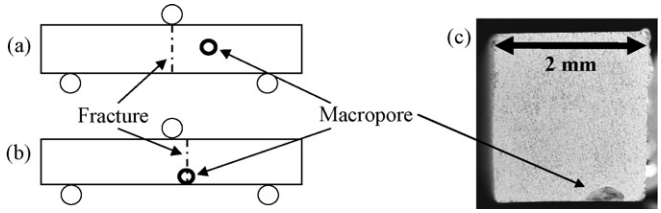

Fig. 12. (a and b) Setup of three-point bending tests and (c) fractograph of a specimen.

$$\sigma_r = \frac{K_{IC}}{Y \cdot \sqrt{a_{C0}g(p_{macro})}} = \{K_{IC0} \cdot [N_C \cdot (1 - p_{micro}) - (N_C - 1) \cdot (1 - p_{micro})^{2/3}] + K_{IC\,min}\} \cdot \frac{(1 - p_{macro})^m}{Y \cdot \sqrt{a_{C0}g(p_{macro})}} \quad (14)$$

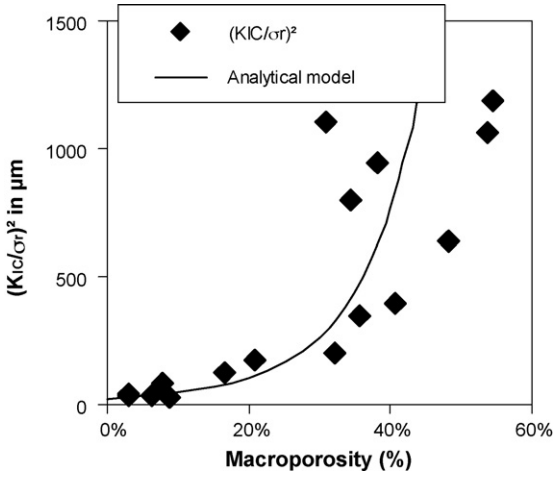

Fig. 13. Variation of $(K_{IC}/\sigma_r)^2$ as function of macroporosity.

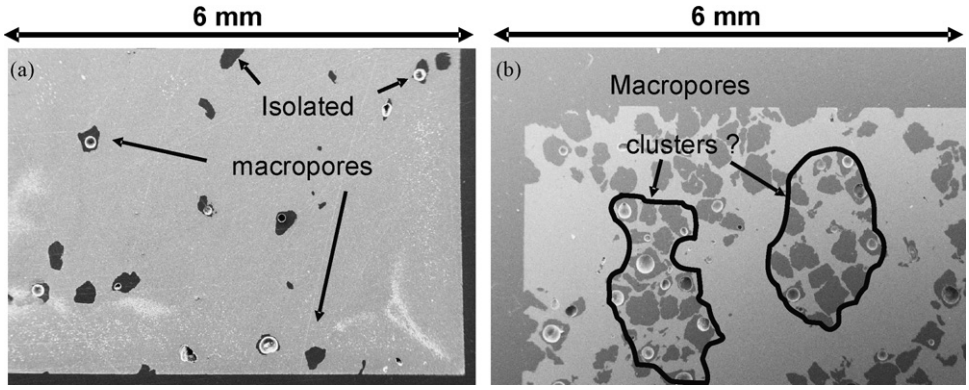

Fig. 14. SEM images of epoxy resin impregnated samples: (a) $p_{macro} = 3.1\%$ and (b) $p_{macro} = 31\%$.

and:

$$\sigma_r = \{\sigma_{r0}[N_C \cdot (1 - p_{micro}) - (N_C - 1) \cdot (1 - p_{micro})^{2/3}] + \sigma_{r\,min}\} \cdot \frac{(1 - p_{macro})^m}{\sqrt{g(p_{macro})}} \quad (15)$$

If, additionally, we assume arbitrarily that the function g can be of the empirical form $(1 - p_{macro})^{-2n}$ (if n is positive, a_C increases with macroporosity, as observed) then the fracture strength model becomes:

$$\sigma_r = \{\sigma_{r0}[N_C \cdot (1 - p_{micro}) - (N_C - 1) \cdot (1 - p_{micro})^{2/3}] + \sigma_{r\,min}\} \cdot (1 - p_{macro})^{m+n} \quad (16)$$

This explains why our data can still be described by a model of the same mathematical form, but with a higher exponent for the macroporosity factor than in the case of toughness. In the present case (batch A), since the fitted values are $m = 2.5$ (for toughness) and $m + n = 5$ (for strength), then n would be equal to 2.5. From a physical point of view, a simple interpretation can be proposed to explain this increase in the critical flaw size with macroporosity. When there is only a limited number of macropores in the specimen (low macroporosity), macropores are quite scattered in the ceramic and do not interact with each other (Fig. 14a). When macroporosity increases, the average distance between neighbouring macropores decreases, and their associated stress concentration fields start to interact. Additionally, from a purely statistical point of view related to the total number of macropores, the probability to find groups of macropores in some areas increases. These groups of macropores can constitute weakened zones of the material, and act as a new enlarged critical flaw instead of a single macropore (Fig. 14b). Such groups of macropores can become critical flaws through subcritical microcrack growth and linking before reaching the peak stress, which is consistent with previously published approaches in other materials.[46,52] As macroporosity increases, these groups of macropores will statistically become larger, which corresponds to the observed progressive increase in critical flaw size. Besides, the role of clusters of pores on the initiation of fracture in brittle materials has already been investigated by numerical approaches. For instance, using a two-dimensional object-oriented finite element code, Cannillo et al. have shown that groups of pores act as local stress concentrators.[46] The consequence is that the global strain at which fracture initiation occurs (and hence the strength) decreases as the distance between pores decreases. As an example, the computed strain at fracture decreases by ~20% when pores are clustered compared to a regular array of pores.

As a matter of verification of our general modelling methodology, and in particular of the transition from a Young's modulus model to a fracture strength model, fractographic observation was undertaken by scanning electron microscopy. First, fractographs did not show any visible difference in rupture micromechanisms between all the specimens sintered at a same temperature (*i.e.* with similar microporosities), whatever their macroporosity is. On the other hand, differences were found between ceramics sintered at different temperatures (*i.e.* with different microporosities). Indeed, specimens sintered at 900 °C during 8 h (high microporosity, 43%) show numerous small ceramic grains (smaller than two micrometers in size), that seem rough, close to elongated spheres in shape and linked to their neighbours by small sintering necks (Fig. 15a). Fracture occurs by decohesion along these very brittle sintering necks, and is therefore completely intergranular. The fracture of specimens sintered at 1000 and 1050 °C during 8 h (intermediate microporosities, 26% and 15% respectively) is displayed in Fig. 15b and c, and exhibit different features. If the sintering necks between adjacent grains still seem to brake in an intergranular manner, a few "continuous blocks" of up to 20 μm (probably made of several grains) show a transgranular fracture behaviour. This transition from intergranular to transgranular fractures is common among many ceramic materials.[53,54] The last fractograph displayed (Fig. 15d) shows the rupture surface of a specimen sintered at 1150 °C that is almost completely dense (with microporosity lower than 5%). Fracture seems mainly intergranular again, as indicated by the presence of well facetted grains on the rupture surface. Even if this phenomenon is not usually described and explained by the literature, it can be observed on fractographies of some dense ceramics (sintered during several hours at high temperatures) published in the past.[11,19,55] From the modelling point of view, the equivalence between the Young's modulus model and the toughness model is valid if the strain to fracture is independent of porosity.[40] It has

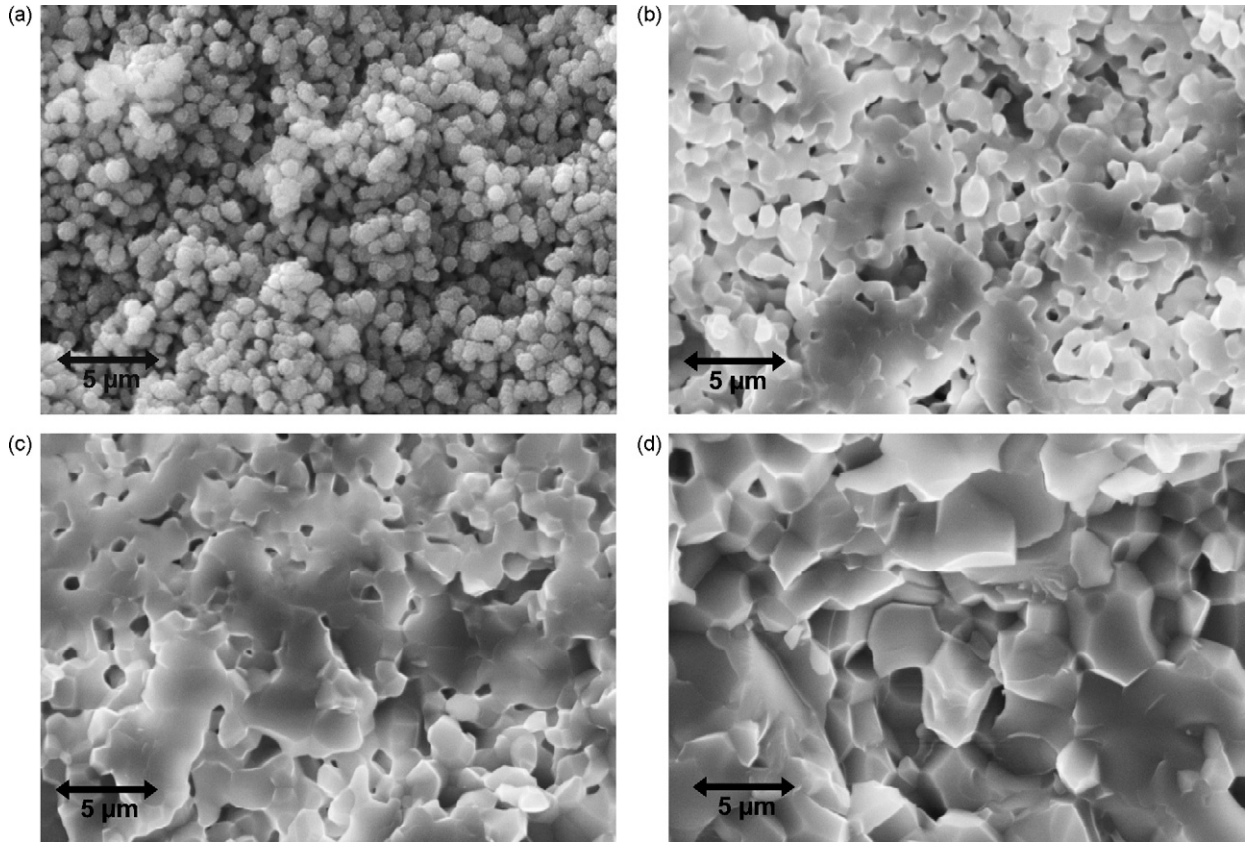

Fig. 15. Fractographs of toughness specimens sintered during 8 h at (a) 900 °C (p_{micro} = 43%), (b) 1000 °C (p_{micro} = 26%), (c) 1050 °C (p_{micro} = 15%) and (d) 1150 °C (p_{micro} = 2%).

been suggested and verified that this is true when the fracture micromechanisms remain the same over the whole range of porosity.[42] It was also observed that, if a change in fracture micromechanisms occurs when porosity changes, this could provoke a variation of the reference toughness, K_{IC0}, with porosity, and hence non-monotonic variations of the fracture energy with porosity.[56] Nevertheless, the condition can be regarded as sufficient, but not necessary. Indeed, in our case, it seems that the observed double transition in fracture mechanisms (from intergranular to mixed and to intergranular again) does not affect the reference value K_{IC0}, since the measured variations are well described by the model, without the need to change K_{IC0}.

5. Conclusion and perspectives

The mechanical properties of BCP ceramics exhibiting actual implant microstructures have been measured over a wide range of porosity. The variations of Young's modulus, fracture toughness and fracture strength of these biomaterials have been described with analytical models as functions of macroporosity and microporosity separately, taking into account their different morphology. Existing models have been adapted to the presently investigated bioceramics. The results indicate that the mechanical behaviour of BCP ceramics can be described by such models, keeping the same set of parameters N_C and m for Young's modulus and toughness, as expected from published theories. Nevertheless, the initial strength model had been built on the hypothesis that the critical flaw is always an isolated macropore, of similar size and shape, which would give the same parameters N_C and m as for the other two properties. On the basis of experimental results, this hypothesis has been rejected, since the parameter m is much higher for strength than for Young's modulus and toughness. This indicates that the critical flaw size increases with macroporosity. A new hypothesis is thus proposed, suggesting that a group of macropores can act as the critical flaw, possibly after subcritical microcrack growth and macropore linking before the peak stress is reached. This is consistent with measurements and experimental observations, although no direct evidence exists so far. One of the perspectives of this work is therefore to introduce voluntarily groups of macropores of different sizes and to evaluate their impact on mechanical properties.

However, even if rather well adapted to describe the collected data, the proposed models still have some limitations: (i) they are not fully predictive since their parameters need to be adjusted to at least a few measurements; (ii) there is no direct observation of the role of (groups of) macropores as critical flaws, although our hypothesis is supported by a set of experimental observations and by existing literature on other materials; (iii) the variation of fracture micromechanisms with microporosity is not taken into account, although it does not seem, at first, to have a significant influence on the evolution fracture properties with porosity; (iv) the fitted value for X_{min} for all properties is of the order of 1% of X_0, which is much smaller than the typical measurement error bar

and would make it non-mandatory to obtain a good description of data (even if X_{min} has a real physical meaning).

Anyway, data description is rather good, and these validated analytical models can then be useful in view of predicting the mechanical behaviour of microporous and macroporous materials on the basis of a few tests only. Eventually, a good understanding of the influence of microstructure on mechanical properties will allow to design bioceramics with optimised performance.

References

1. Albee, F. H., Studies in bone growth: triple calcium phosphate as a stimulus to osteogenesis. *Annals of Surgery*, 1920, **71**, 32.
2. Cavagna, R., Daculsi, G. and Bouler, J. M., Macroporous calcium phosphate ceramic: a prospective study of 106 cases in lumbar spinal fusion. *Journal of Long-Term Effects of Medical Implants*, 1999, **9**, 403–412.
3. Gouin, F., Delécrin, J., Passuti, N., Touchais, S., Poirier, P. and Bainvel, J. V., Comblements osseux par céramique phosphocalcique biphasée macroporeuse. A propos de 23 cas. *Revue de Chirurgie Orthopédique et Réparatrice de l'Appareil Moteur*, 1995, **81**, 59–65.
4. Kraal, T., Mullender, M., De Bruine, J. H. D., Reinhard, R., De Gasta, A., Kuikc, D. J. *et al.*, Resorbability of rigid beta-tricalcium phosphate wedges in open-wedge high tibial osteotomy: a retrospective radiological study. *The Knee*, 2008, **15**, 201–205.
5. Ransford, A. O., Morley, T., Edgar, M. A. and Webb, P., Synthetic porous ceramic compared with autograft in scoliosis surgery: a prospective, randomised study of 341 patients. *Journal of Bone and Joint Surgery (British)*, 1998, **80-B**, 13–18.
6. Rey, C., Calcium phosphate biomaterials and bone mineral. Differences in composition, structures and properties. *Biomaterials*, 1990, **11**, 13–15.
7. Sillen, A. and LeGeros, R., Solubility profiles of synthetic apatites and of modern and fossil bones. *Journal of Archaeological Science*, 1991, **18**, 385–397.
8. Yamada, S., Heymann, D., Bouler, J. M. and Daculsi, G., Osteoclastic resorption of calcium phosphate ceramics with different hydroxyapatite/β-tricalcium phosphate ratios. *Biomaterials*, 1997, **18**, 1037–1041.
9. LeGeros, R. Z. and Parsons, J. R., Significance of the porosity and physical chemistry of calcium phosphate ceramics biodegradation–bioresorption. *Annals of the New York Academy of Sciences*, 1988, **523**, 268–271.
10. LeGeros, R. Z., Biodegradation and bioresorption of calcium phosphate ceramics. *Clinical Materials*, 1993, **14**, 65–88.
11. Ruseska, G., Fidanceska, E. and Bossert, J., Mechanical and thermal-expansion characteristics of $Ca_{10}(PO_4)_6(OH)_2$-$Ca_3(PO_4)_2$. *Science of Sintering*, 2006, **38**, 245–254.
12. Gauthier, O., Bouler, J. M., Aguado, E., Pilet, P. and Daculsi, G., Macroporous biphasic calcium phosphate ceramics: influence of macropore diameter and macroporosity percentage on bone ingrowth. *Biomaterials*, 1998, **19**, 133–139.
13. Bouler, J. M., Trécant, M., Delécrin, J., Royer, J., Passuti, N. and Daculsi, G., Macroporous biphasic calcium phosphate ceramics: influence of five synthesis parameters on compressive strength. *Journal of Biomedical Materials Research*, 1996, **32**.
14. De Groot, K., Effect of porosity and physicochemical properties on the stability, resorption, and strength of calcium phosphate ceramics. *Annals of the New York Academy of Sciences*, 1988, **523**, 227–233.
15. Raynaud, S., Champion, E., Lafon, J. P. and Bernache-Assollant, D., Calcium phosphate apatites with variable Ca/P atomic ratio III. Mechanical properties and degradation in solution of hot pressed ceramics. *Biomaterials*, 2002, **23**, 1081–1089.
16. Veljovic, Dj., Jokić, B., Petrović, R., Palcevskis, E., Dindune, A., Mihailescu, I. N. *et al.*, Processing of dense nanostructured HAP ceramics by sintering and hot pressing. *Ceramics International*, 2009, **35**, 1407–1413.
17. Bouslama, N., Ben Ayed, F. and Bouaziz, J., Effect of fluorapatite additive on densification and mechanical properties of tricalcium phosphate. *Journal of the Mechanical Behavior of Biomedical Materials*, in press [doi:10.1016/j.jmbbm.2009.01.007, corrected proof].
18. Landi, E., Celotti, G., Logroscino, G. and Tampieri, A., Carbonated hydroxyapatite as bone substitute. *Journal of the European Ceramic Society*, 2003, **23**, 2931–2937.
19. Thangamani, N., Chinnakali, K. and Gnanam, F. D., The effect of powder processing on densification, microstructure and mechanical properties of hydroxyapatite. *Ceramics International*, 2002, **28**, 355–362.
20. Zhang, Y., Xu, H. H. K., Takagi, S. and Chow, L. C., In situ hardening hydroxyapatite-based scaffold for bone repair. *Journal of Materials Science: Materials in Medicine*, 2006, **17**, 437–445.
21. Milosevski, M., Bossert, J., Milosevski, D. and Gruevska, N., Preparation and properties of dense and porous calcium phosphate. *Ceramics International*, 1999, **25**, 693–696.
22. Bignon, A., Chouteau, J., Chevalier, J., Fantozzi, G., Carret, J. P., Chavassieux, P. *et al.*, Effect of micro-and macroporosity of bone substitutes on their mechanical properties and cellular response. *Journal of Materials Science: Materials in Medicine*, 2003, **14**, 1089–1097.
23. Le Huec, J. C., Schaeverbeke, T., Clement, D., Faber, J. and Le Rebeller, A., Influence of porosity on the mechanical resistance of hydroxyapatite ceramics under compressive stress. *Biomaterials*, 1995, **16**, 113–118.
24. Dewey, J. M., The elastic constants of materials loaded with non-rigid fillers. *Journal of Applied Physics*, 1947, **18**, 578–581.
25. Wagner, P., O'Rourke, J. A. and Armstrong, P. E., Porosity effects in polycrystalline graphite. *Journal of the American Ceramic Society*, 1972, **55**, 214–219.
26. Christensen, R. M., Mechanics of cellular and other low-density materials. *International Journal of Solids and Structures*, 2000, **37**, 93–104.
27. Eshelby, J. D., The determination of the elastic field of an ellipsoidal inclusion, and related problems. *Proceedings of the Royal Society of London. Series A, Mathematical and Physical Sciences*, 1957, **241**, 376–396.
28. Hashin, Z. and Shtrikman, S., On some variational principles in anisotropic and nonhomogeneous elasticity. *Journal of the Mechanics and Physics of Solids*, 1962, **10**, 335–342.
29. Budiansky, B., On the elastic moduli of some heterogeneous materials. *Journal of the Mechanics and Physics of Solids*, 1965, **13**, 223–227.
30. Boccaccini, A. R. and Fan, Z., A new approach for the Young's modulus-porosity correlation of ceramic materials. *Ceramics International*, 1997, **23**, 239–245.
31. Hasselman, D. P. H., On the porosity dependence of the elastic moduli of polycrystalline refractory materials. *Journal of the American Ceramic Society*, 1962, **45**, 452–453.
32. Ramakrishnan, N. and Arunachalam, V. S., Effective elastic moduli of porous solids. *Journal of Materials Science*, 1990, **25**, 3930–3937.
33. Gibson, L. J. and Ashby, M. F., The mechanics of three-dimensional cellular materials. *Proceedings of the Royal Society of London. Series A. Mathematical and Physical Sciences*, 1982, **382**, 43–59.
34. Munro, R. G., Effective medium theory of the porosity dependence of bulk moduli. *Journal of the American Ceramic Society*, 2001, **84**, 1190–1192.
35. Phani, K. K. and Niyogi, S. K., Young's modulus of porous brittle solids. *Journal of Materials Science*, 1987, **22**, 257–263.
36. Rice, R. W., *Mechanical Properties of Ceramics and Composites: Grain and Particle Effects*. CRC Press, 2000.
37. Rice, R. W., Evaluation and extension of physical property-porosity models based on minimum solid area. *Journal of Materials Science*, 1996, **31**, 102–118.
38. Jernot, J. P., Coster, M. and Chermant, J. L., Model to describe the elastic modulus of sintered materials. *Physica Status Solidi (a)*, 1982, **72**.
39. Wagh, A. S., Poeppel, R. B. and Singh, J. P., Open pore description of mechanical properties of ceramics. *Journal of Materials Science*, 1991, **26**, 3862–3868.
40. Wagh, A. S., Singh, J. P. and Poeppel, R. B., Dependence of ceramic fracture properties on porosity. *Journal of Materials Science*, 1993, **28**, 3589–3593.
41. Arató, P., Comment on "dependence of ceramics fracture properties on porosity". *Journal of Materials Science Letters*, 1996, **15**, 32–33.
42. Tancret, F., Desgardin, G. and Osterstock, F., Influence of porosity on the mechanical properties of cold isostatically pressed and sintered

$YBa_2Cu_3O_{7-x}$ superconductors. *Philosophical Magazine A*, 1997, **75**, 505–523.
43. Keum, Y. T. and Oh, J. W., Finite element simulation of a ceramic drying process considering pore shape and porosity. *Modelling and Simulation in Materials Science and Engineering*, 2005, **13**, 225–237.
44. Tessier-Doyen, N., Etude expérimentale et numérique du comportement thermomécanique de matériaux réfractaires modèles. PhD thesis. Université de Limoges, France, 2003.
45. Roberts, A. P. and Garboczi, E. J., Elastic properties of model random three-dimensional open-cells solids. *Journal of the Mechanics and Physics of Solids*, 2002, **50**, 33–55.
46. Cannillo, V., Leonelli, C., Manfredini, T., Montorsi, M. and Boccaccini, A. R., Use of numerical approaches to predict mechanical properties of brittle bodies containing controlled porosity. *Journal of Materials Science*, 2004, **39**, 4335–4337.
47. Schneider, T., Greil, P. and Schober, G., Strength modeling of brittle materials with two- and three-dimensional pore structures. *Computational Materials Science*, 1999, **16**, 98–103.
48. Tancret, F., Bouler, J. M., Chamousset, J. and Minois, L. M., Modelling the mechanical properties of microporous and macroporous biphasic calcium phosphate bioceramics. *Journal of the European Ceramic Society*, 2006, **26**, 3647–3656.
49. Friel, J. J., *Practical Guide to Image Analysis*. ASTM International, Materials Park, 1992, pp. 101–128.
50. Dlouhy, I., Holzmann, M., Man, J. and Valka, L., The use of chevron notched specimen for fracture toughness determination. *Metallic Materials*, 1994, **32**, 3–13.
51. Krstic, V. D., Effect of microstructure on fracture of brittle materials: unified approach. *Theoretical and Applied Fracture Mechanics*, 2006, **45**, 212–226.
52. Pernot, F., Etienne, P., Boschet, F. and Datas, L., Weibull parameters and the tensile strength of porous phosphate glass-ceramics. *Journal of the American Ceramic Society*, 1999, **82**, 641–648.
53. Deng, Z., Fukasawa, T., Ando, M., Zhang, G. J. and Ohji, T., Microstructure and mechanical properties of porous alumina ceramics fabricated by the decomposition of aluminum hydroxide. *Journal of the American Ceramic Society*, 2001, **84**, 2638–2644.
54. Harabia, A. and Davies, T., Mechanical properties of sintered alumina–chromia refractories. *British Ceramic Transactions*, 1995, **94**, 79–84.
55. Chanda, P. K., Ono, M., Kuwano, M. and Kung, H., Microwave sintering of calcium phosphate ceramics. *Materials Science and Engineering: C*, 2009, **29**, 1144–1149.
56. Tancret, F. and Osterstock, F., Modelling the toughness of porous sintered glass beads with various fracture mechanisms. *Philosophical Magazine*, 2003, **83**, 137–150.